



## In vitro corrosion behavior and in vivo biodegradation of biomedical $\beta$ - $\text{Ca}_3(\text{PO}_4)_2/\text{Mg-Zn}$ composites

Kun Yu<sup>a,c</sup>, Liangjian Chen<sup>b,c,\*</sup>, Jun Zhao<sup>a</sup>, Shaojun Li<sup>a</sup>, Yilong Dai<sup>a</sup>, Qiao Huang<sup>a</sup>, Zhiming Yu<sup>a</sup>

<sup>a</sup> School of Materials Science and Engineering, Central South University, Changsha 410083, People's Republic of China

<sup>b</sup> XiangYa Third Hospital, Central South University, Changsha 410083, People's Republic of China

<sup>c</sup> State Key Laboratory of Powder Metallurgy, Changsha 410083, People's Republic of China

### ARTICLE INFO

#### Article history:

Received 21 November 2011

Received in revised form 17 March 2012

Accepted 3 April 2012

Available online 11 April 2012

#### Keywords:

Composite

Corrosion product

Simulated body fluid

Mechanical properties

Cytotoxicity

### ABSTRACT

In this study 5, 10 and 15%  $\beta$ - $\text{Ca}_3(\text{PO}_4)_2/\text{Mg-Zn}$  composites were prepared through powder metallurgy methods, and their corrosion behavior and mechanical properties were studied in simulated body fluid (SBF) at 37 °C. The 10%  $\beta$ - $\text{Ca}_3(\text{PO}_4)_2/\text{Mg-Zn}$  composite was selected for cytocompatibility assessment and in vivo biodegradation testing. The results identified the  $\alpha$ -Mg, MgZn and  $\beta$ - $\text{Ca}_3(\text{PO}_4)_2$  phases in these sintered composites. The density and elastic modulus of the  $\beta$ - $\text{Ca}_3(\text{PO}_4)_2/\text{Mg-6% Zn}$  composite match those of natural bone, and the strength is approximately double that of natural bone. The 10%  $\beta$ - $\text{Ca}_3(\text{PO}_4)_2/\text{Mg-6% Zn}$  composites exhibit good corrosion resistance, as determined by a 30 day immersion test and electrochemical measurements in SBF at 37 °C. The 10%  $\beta$ - $\text{Ca}_3(\text{PO}_4)_2/\text{Mg-6% Zn}$  composite is safe for cellular applications, with a cytotoxicity grade of ~0–1 against L929 cells in in vitro testing. The  $\beta$ - $\text{Ca}_3(\text{PO}_4)_2/\text{Mg-6% Zn}$  composite also exhibits good biocompatibility with the tissue and the important visceral organs the heart, kidney and liver of experimental rabbits. The composite has a suitable degradation rate and improves the concrecence of a pre-broken bone. The corrosion products, such as  $\text{Mg}(\text{OH})_2$  and  $\text{Ca}_5(\text{PO}_4)_6(\text{OH})_2$ , can improve the biocompatibility of the  $\beta$ - $\text{Ca}_3(\text{PO}_4)_2/\text{Mg-Zn}$  composite.

© 2012 Acta Materialia Inc. Published by Elsevier Ltd. All rights reserved.

### 1. Introduction

Biomedical metals and alloys are widely used for joint and bone implants because of their good physical properties, such as strength, toughness, ductility and corrosion resistance [1]. The typical biomedical metals and alloys used for implants include stainless steels and Ti-based, Co-based, Ni-based and Ta-based alloys [2]. These materials can be fabricated into plates, screws and pins to repair serious bone fractures or to assist in the healing process, but a second surgical intervention must be performed to remove the metallic implants from the body after the bones or tissues have healed, or they will remain there permanently [3,4]. The need for additional surgery increases the patient suffering. In contrast, biodegradable materials dissolve after the healing process is complete, and no additional surgery is required to remove these implants [5]. These materials also eliminate the complications associated with the long-term presence of implants in the body. Polymers such as polyglycolic acid, polylactic acid and polydioxanone were the first materials used in biodegradable implants. However, these materials are limited by their poor mechanical properties and

radiolucency [1]. Metals and alloys have desirable mechanical properties because of their relatively high strength, but studies have shown that conventional surgical alloys produce corrosion products that are harmful to the human body [2,3]. On the other hand, magnesium and its corrosion products have excellent biocompatibility, and thus Mg has garnered significant attention as a biomaterial for temporary medical implants [6].

Magnesium and its alloys are light weight metal materials with mechanical properties similar to those of natural bone [3]. The elastic modulus of Mg-based implants matches with that of cortical bone tissue, so it can avoid the stress shielding effect induced by a serious mismatch between the modulus of natural bone and other metal implants [7]. Mg-based implants corrode when in contact with body fluid, with the degradation occurring via corrosion in the electrolytic physiological environment [8,9]. This finding implies that Mg alloys have the potential to serve as biodegradable implants because they form non-toxic corrosion products with an appropriate pH level in the high chloride environment of physiological systems. Hence, it is important to study the in vitro corrosion behavior and in vivo biocompatibility of Mg-based implants.

Many previous investigations have studied the properties of different Mg alloys as candidates for biodegradable materials in the orthopedic field [10,11]. The properties, biological performance and challenges of magnesium and its alloys as orthopedic biomaterials have also been summarized in review articles [8,12]. In vitro

\* Corresponding author at: XiangYa Third Hospital, Central South University, Changsha 410083, People's Republic of China. Tel.: +86 731 88879341; fax: +86 731 88876692.

E-mail address: [yukungroup@gmail.com](mailto:yukungroup@gmail.com) (L. Chen).

and in vivo corrosion studies of some typical magnesium alloys, such as AZ31, AZ91, WE43 and LAE442, have been reported; the results provide a strong rationale for using magnesium alloys as future implant materials in bone surgery [11,13,14]. Some biodegradable Mg–Zn, Mg–Ca, Mg–Si and Mg–Mn alloys have also been tested in simulated physiological environments [15]. However, current research indicates that there is a high demand for Mg alloys with adjustable corrosion rates to meet the requirements of bone replacement or repair, because the corrosion rates of many commercial Mg alloys are too rapid to allow sufficient time for healing (at least 12 weeks). Although the Mg–Al and Mg–rare earth system alloys demonstrate improved corrosion resistance, they contain aluminum and rare earth elements, which are harmful to human health [16,17]. One alternative is the application of Mg-based metal matrix composites (MMCs) [18]. The advantages of Mg-based MMCs as biomaterials include their appropriate mechanical properties and an adjustable corrosion rate, where the latter can be controlled by choosing the category and content of the reinforcement. Like hydroxyapatite,  $\beta$ - $\text{Ca}_3(\text{PO}_4)_2$  can biodegrade in bodily fluids and can be used as a reinforcement in Mg-based alloys to fabricate biocomposites [19]. There are no previous reports of  $\beta$ - $\text{Ca}_3(\text{PO}_4)_2$  particles used as reinforcements in a Mg alloy matrix to fabricate an MMC. Hence, in this study different percentages of  $\beta$ - $\text{Ca}_3(\text{PO}_4)_2$  particles are added to reinforce a Mg–6% Zn alloy in order to design a new biomedical material candidate. A Mg–6% Zn alloy was selected as the matrix because it has high strength and good corrosion resistance, in addition to its non-toxic elemental composition. The alloying element zinc has a direct effect on bone mineralization and may stimulate bone formation in the tissue [20]. Therefore, the in vitro corrosion properties of  $\beta$ - $\text{Ca}_3(\text{PO}_4)_2$ /Mg–6% Zn composites in simulated body fluid at the physiological ambient temperature of 37 °C were studied first. Then the cytocompatibility of this experimental MMC were evaluated, and the in vivo biodegradation and biocompatibility of this MMC with animal bone studied. Taken together, these investigations aimed to develop a biomaterial candidate that meets the biocompatibility and biodegradability demands of medical implants.

## 2. Materials and methods

### 2.1. Material production

The  $\beta$ - $\text{Ca}_3(\text{PO}_4)_2$  powder was produced through a solid calcination reaction of commercial  $\text{CaHPO}_4$  and  $\text{CaCO}_3$  powders at 950–960 °C for 4 h. The chemical reaction proceeded as follows [21]:



The average particle size of the obtained  $\beta$ - $\text{Ca}_3(\text{PO}_4)_2$  powder was 7.85  $\mu\text{m}$ , as determined using a Micro-Plus laser particle size analyzer.

The experimental MMC specimens were prepared using the powder metallurgy method. The matrix composition of the experimental composite was Mg–6% Zn (wt.%), with 5, 10 and 15 wt.%  $\beta$ - $\text{Ca}_3(\text{PO}_4)_2$  particles added. As a control specimen a Mg–6% Zn alloy with no reinforcing material was also prepared in the same way. The average particle diameter of the Mg and Zn powders used in the experiment was 23.0  $\mu\text{m}$ , and the purity was greater than 99.95%. The Mg, Zn and  $\beta$ - $\text{Ca}_3(\text{PO}_4)_2$  powders were mixed together in a vacuum tank for 1 h. The mixed powders were cold pressed to a billet and sintered at 620–640 °C for 2 h in a vacuum sinter furnace under argon gas. The diameter of the sintered  $\beta$ - $\text{Ca}_3(\text{PO}_4)_2$ /Mg–6% Zn MMC billets was 64 mm, and the thickness was 18 mm. All of the experimental specimens for mechanical properties testing,

in vitro corrosion testing and in vivo measurements were cut from the sintered composite billets. Three samples of each of the MMCs were tested in each experiment and the average values are presented as the results.

### 2.2. Mechanical and metallurgical testing

The densities of the specimens were measured and calculated using the Archimedes principle and an electronic balance. The compression strengths and elastic moduli of the experimental  $\beta$ - $\text{Ca}_3(\text{PO}_4)_2$ /Mg–6% Zn specimens were measured in a Gleeble 1500 thermo-mechanical simulator machine at 37 °C. Specimens for mechanical testing with a diameter of 10 mm and a thickness of 15 mm were cut from the sintered billets. The Brinell hardness was tested with a standard HW187.5 hardness tester. The microstructures of the experimental MMCs were observed with a Polar-MET metallographic microscope and a JEOL JSM-5600Lv scanning electron microscope with an energy-dispersive X-ray spectroscope. Phase identification of the corrosion products of the specimens was performed using a DMAX-2500X X-ray diffractometer using  $\text{CuK}_\alpha$  radiation with a wavelength of 1.5406 Å.

### 2.3. In vitro corrosion testing

The in vitro corrosion tests included immersion testing and electrochemical testing. The specimens for the corrosion test were ground with 1000 grid SiC sandpaper and cleaned with ethanol. Immersion corrosion testing under static conditions was performed in simulated body fluid (SBF) at 37 ± 0.2 °C for 30 days. The SBF was a solution of recently boiled distilled water containing 8.6 g of sodium chloride, 0.3 g of potassium chloride, and 0.33 g of calcium chloride per liter [2,3]. The SBF was not stirred during the experiments and was saturated with atmospheric oxygen. The corrosion rates were determined by weight loss measurements performed using chromic acid to remove the corrosion products. The SBF temperature was controlled with an HTW-10B water bath.

The electrochemical testing was performed in SBF at 37 °C with a CHI660D potentiostat/galvanostat system. The electrochemical properties were measured in a three electrode configuration: the experimental MMC was the working electrode, the reference electrode was a saturated calomel electrode (SCE), and the counter-electrode was a platinum plate. The specimen size for the immersion test was 20 × 20 × 10 mm, and the testing area of the electrochemical testing specimen was 100 mm<sup>2</sup>. The change in the pH value of the SBF after corrosion testing was determined using a Mettler Toledo FE20 pH sensor.

### 2.4. Cytocompatibility assessments

The cytotoxicity of the materials was measured via indirect contact testing according to ISO 10993-5:1999. The experimental MMC specimens were immersed in 10% fetal bovine serum in an incubator at 95% relative humidity and 5% CO<sub>2</sub> at 37 °C. L-929 cells were cultured in Dulbecco's modified Eagle's medium (DMEM). The culture medium was replaced by 100% extraction medium or 50 or 10% dilutions. The DMEM acted as a negative control, and a sample of the DMEM medium containing phenol acted as a positive control. 3-(4,5-Dimethylthiazol-2-yl)-2,5-diphenyltetrazolium bromide (MTT) was then dissolved in phosphate-buffered saline (PBS) at a concentration of 5 mg ml<sup>-1</sup>. The samples were incubated for 4 h after adding 10  $\mu\text{l}$  of the MTT solution. Subsequently, 100 ml of formazan solution was added to each sample, and the optical density (OD) was measured using a spectrophotometer. The cell relative growth rate (RGR) was calculated as follows:

$$\text{RGR} = \text{OD}_{\text{test}} / \text{OD}_{\text{negative}} \times 100\%$$

### 2.5. In vivo biocompatibility and degradation testing

All animal experiments were performed according to the animal welfare legislation of the People's Republic of China and approved by the Ethics Committee of the Xiangya Third Hospital. In total, eight adult male Zelanian rabbits with a body weight of ~2.0–2.5 kg were randomly assigned to two groups. In the treatment group  $5 \times 5 \times 2$  mm samples were produced from the experimental MMCs and implanted into the dorsal muscles of the animals. A of  $12 \times 5 \times 2$  mm splint was machined from the experimental MMCs and fastened to an animal's pre-broken femoral shaft. In the control group each rabbit had a fracture in the femoral shaft without any implantation. All rabbits were anesthetized with amyl-barbiturate ( $30 \text{ mg kg}^{-1}$ ) for surgery. Post-operatively the Zelanian rabbits were allowed to move freely in their cages. Venous blood samples from the rabbits were phlebotomized from 1 day to 12 weeks at different times to detect the variations in Mg, Zn, and Ca ion concentrations in the blood. The animals were killed 12 weeks after surgery. A histological evaluation was performed on hematoxylin and eosin (HE) stained sections. The muscle tissue around the implanted MMC and tissue from the heart, liver and kidneys of the rabbits were also inspected with HE staining for histomorphology analysis and to detect whether degradation of the experimental MMCs harmed these important visceral organs. Microcomputed tomography (micro-CT) devices were used to observe the in vivo degradation process after implant fixation.

## 3. Results

### 3.1. Mechanical and metallurgical characterization

The metallographic microstructure of the Mg–6% Zn matrix alloy and the  $\beta\text{-Ca}_3(\text{PO}_4)_2/\text{Mg}$ –6% Zn composites with the addition of 5, 10 or 15%  $\beta\text{-Ca}_3(\text{PO}_4)_2$  are shown in Fig. 1. The powder

metallurgy method is one of the best methods for MMC preparation, and the  $\beta\text{-Ca}_3(\text{PO}_4)_2$  particles were successfully retained by the Mg–6% Zn matrix. The three sintered MMC samples had high relative densities and their porosities were all less than 1%. The distribution of  $\beta\text{-Ca}_3(\text{PO}_4)_2$  particles was uniform and dispersed for the samples containing 5 and 10%  $\beta\text{-Ca}_3(\text{PO}_4)_2$ . When the percentage of  $\beta\text{-Ca}_3(\text{PO}_4)_2$  particles was 15% the reinforcement particles agglomerated, with an aggregate size greater than  $30 \mu\text{m}$ . Generally, such conglomerations of  $\beta\text{-Ca}_3(\text{PO}_4)_2$  particles is undesirable for the composite because a heterogeneous distribution of the reinforcement material leads to spatial heterogeneity of its properties. Therefore, selecting a suitable percentage of reinforcing material and ensuring its homogeneous distribution are important in fabricating successful experimental  $\beta\text{-Ca}_3(\text{PO}_4)_2/\text{Mg}$ –6% Zn composites.

Phase identification of  $\beta\text{-Ca}_3(\text{PO}_4)_2/\text{Mg}$ –6% Zn was performed by X-ray diffraction (XRD), and the results are provided in Fig. 2. The main phases in the experimental MMCs are  $\alpha\text{-Mg}$ , intermetallic MgZn and  $\beta\text{-Ca}_3(\text{PO}_4)_2$  phases.

Table 1 summarizes the mechanical properties of the MMC specimens compared with the equivalent properties of natural bone, a typical Ti-based implant alloy and stainless steel. The densities of the three  $\beta\text{-Ca}_3(\text{PO}_4)_2/\text{Mg}$ –6% Zn composites are close to that of natural bone. The elastic modulus is another parameter of the composites that compares favorably with the value of natural bone. Because the elastic modulus can be conveniently modified by changing the percentage of  $\beta\text{-Ca}_3(\text{PO}_4)_2$  particles in the composite, candidate materials can be fabricated according to the different modulus requirements of cortical or cancellous bones. The Brinell hardness values of the experimental MMCs also match that of natural bone. The compressive strengths of the three  $\beta\text{-Ca}_3(\text{PO}_4)_2/\text{Mg}$ –6% Zn specimens were higher than that of natural bone; in particular, the compressive strength of the 5%  $\beta\text{-Ca}_3(\text{PO}_4)_2/\text{Mg}$ –6% Zn specimen was almost twice that of natural bone. Taken together, the measured data show that the  $\beta\text{-Ca}_3(\text{PO}_4)_2/\text{Mg}$ –6% Zn compos-

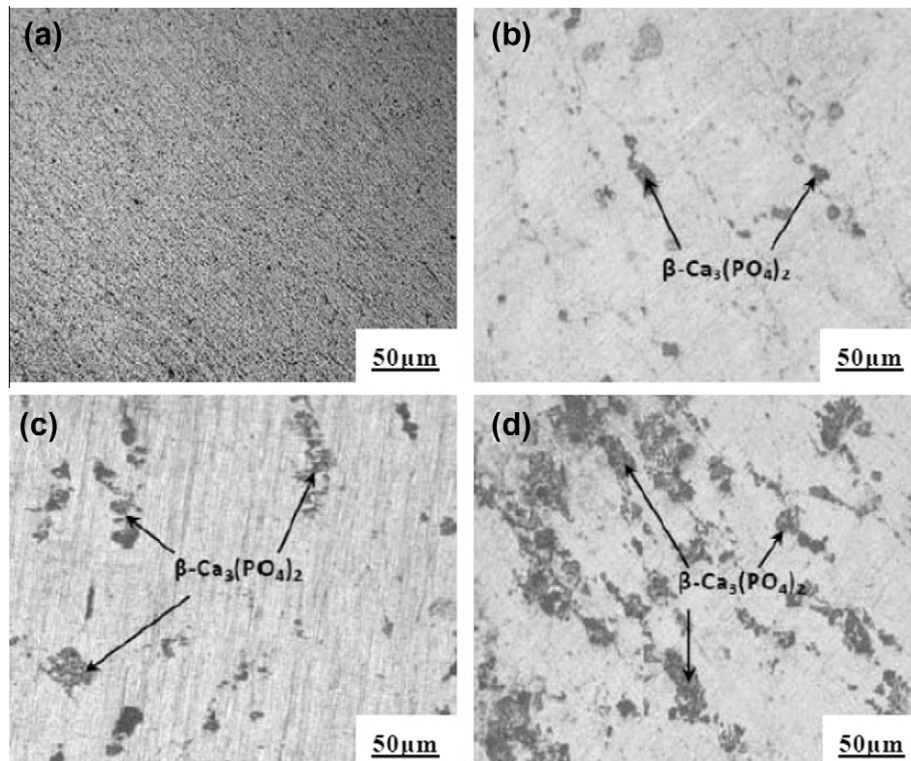


**Fig. 1.** Metallographic microstructures of the sintered specimens. Optical images of (a) Mg–6% Zn alloy, (b) 5%  $\beta\text{-Ca}_3(\text{PO}_4)_2/\text{Mg}$ –6% Zn, (c) 10%  $\beta\text{-Ca}_3(\text{PO}_4)_2/\text{Mg}$ –6% Zn and (d) 15%  $\beta\text{-Ca}_3(\text{PO}_4)_2/\text{Mg}$ –6% Zn.

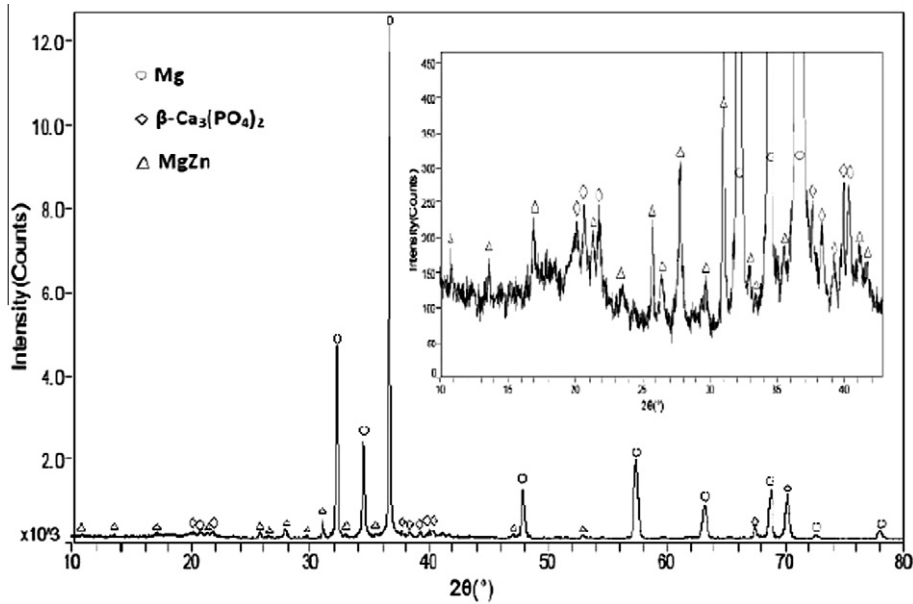


Fig. 2. X-ray identification of the Mg, MgZn and  $\beta$ - $\text{Ca}_3(\text{PO}_4)_2$  phases in the MMC.

**Table 1**  
Mechanical properties of the  $\beta$ - $\text{Ca}_3(\text{PO}_4)_2$ /Mg-6% Zn MMCs compared with other materials.

Material	Density ( $\text{g cm}^3$ )	Brinell hardness	Compressive strength (Mpa)	Elastic modulus (Gpa)
Mg-6% Zn	1.827	67	310	45
5% $\beta$ - $\text{Ca}_3(\text{PO}_4)_2$ /Mg-6% Zn	1.862	39.2	345	36
10% $\beta$ - $\text{Ca}_3(\text{PO}_4)_2$ /Mg-6% Zn	1.904	46.1	339	24
15% $\beta$ - $\text{Ca}_3(\text{PO}_4)_2$ /Mg-6% Zn	1.943	51.2	284	21
Natural bone [2,22]	1.8–2.1	20–58	130–180	3–20
Ti alloy [2,23]	4.4–4.5	70	758–1117	110–117
Stainless steel [2]	7.6–8.3	258–567	480–834	70–230

ites demonstrate mechanical properties comparable with those of natural bone.

### 3.2. Corrosion testing

#### 3.2.1. Immersion testing

Immersion testing of the  $\beta$ - $\text{Ca}_3(\text{PO}_4)_2$ /Mg-6% Zn specimens in SBF is the first step in evaluating the in vitro corrosion behavior of such MMCs. The weight changes of the Mg-6% Zn alloy and the three  $\beta$ - $\text{Ca}_3(\text{PO}_4)_2$ /Mg-6% Zn composites after immersion in SBF at 37 °C for 30 days were measured. Then the corrosion rate or degradation rate of the specimens in SBF determined by the weight loss method was calculated according to [24].

$$CR = \frac{\Delta W}{A \cdot t} \quad (2)$$

where CR is the corrosion rate,  $\Delta W$  is the weight loss from the sample, A is the initial surface area and t is the immersion time. In this experiment the specimens were soaked in an aqueous solution of chromic acid ( $200 \text{ g l}^{-1} \text{ CrO}_3 + 10 \text{ g l}^{-1} \text{ AgNO}_3 + 20 \text{ g l}^{-1} \text{ Ba}(\text{NO}_3)_2$ ) for 5 min to remove the corrosion products. The relationship between the calculated CR values and the immersion times is shown in Fig. 3. The curves reveal that the corrosion rates of all specimens decreased with increasing immersion time. The 5%  $\beta$ - $\text{Ca}_3(\text{PO}_4)_2$ /Mg-6% Zn sample had the lowest corrosion rate, and the Mg-6% Zn alloy showed the highest corrosion rate. The corrosion rate of the 10%  $\beta$ - $\text{Ca}_3(\text{PO}_4)_2$ /Mg-6% Zn sample was slightly higher than that of the 5%  $\beta$ - $\text{Ca}_3(\text{PO}_4)_2$ /Mg-6% Zn sample, and the 15%  $\beta$ - $\text{Ca}_3(\text{PO}_4)_2$ /

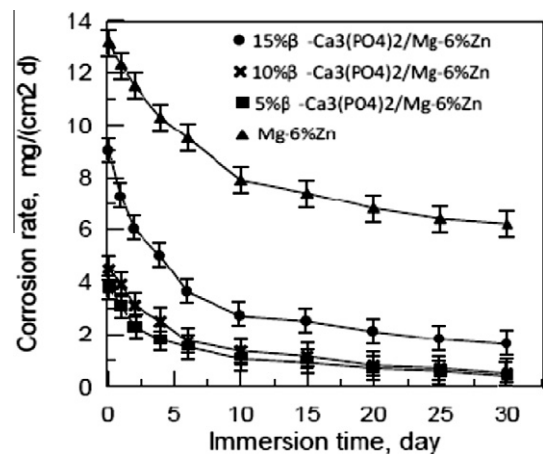


Fig. 3. Calculated corrosion rates of the MMC specimens in SBF.

Mg-6% Zn sample had a corrosion rate that is clearly higher than those of the other two composites. All corrosion rates were high during the first 15 days of the test; subsequently, the corrosion rates decreased slightly over time until the day 30.

Another experimental phenomenon that can be observed in the immersion corrosion testing of  $\beta$ - $\text{Ca}_3(\text{PO}_4)_2$ /Mg-6% Zn specimens is the release of hydrogen gas and the formation of gas bubbles. Visible bubbles of hydrogen gas were released from the specimen surface, especially at the beginning of the immersion period, but

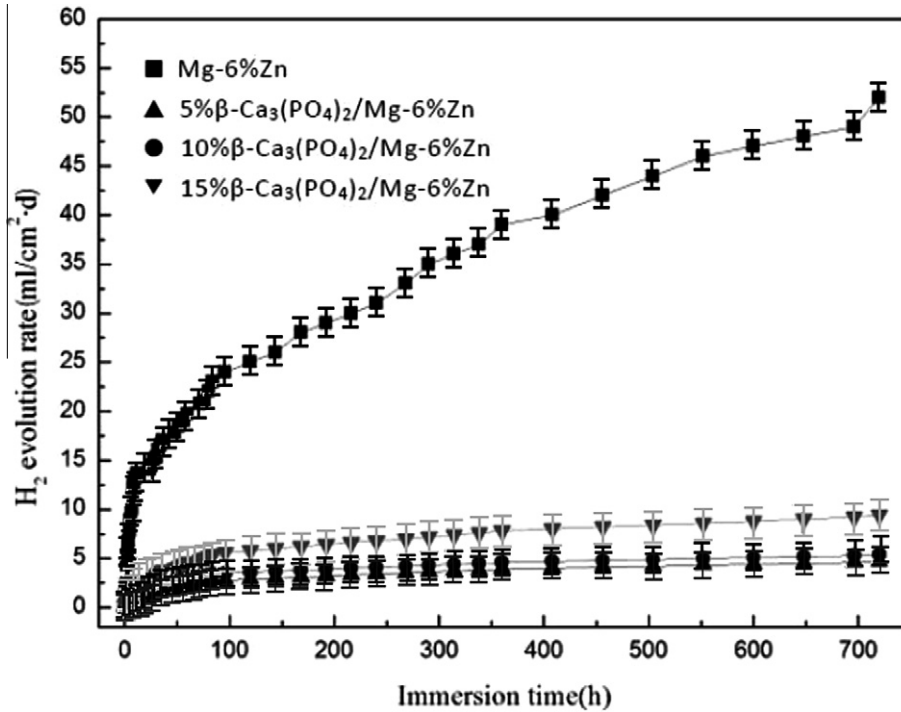


Fig. 4. Hydrogen evolution from the Mg-6% Zn and  $\beta$ -Ca<sub>3</sub>(PO<sub>4</sub>)<sub>2</sub>/Mg-6% Zn specimens in SBF.

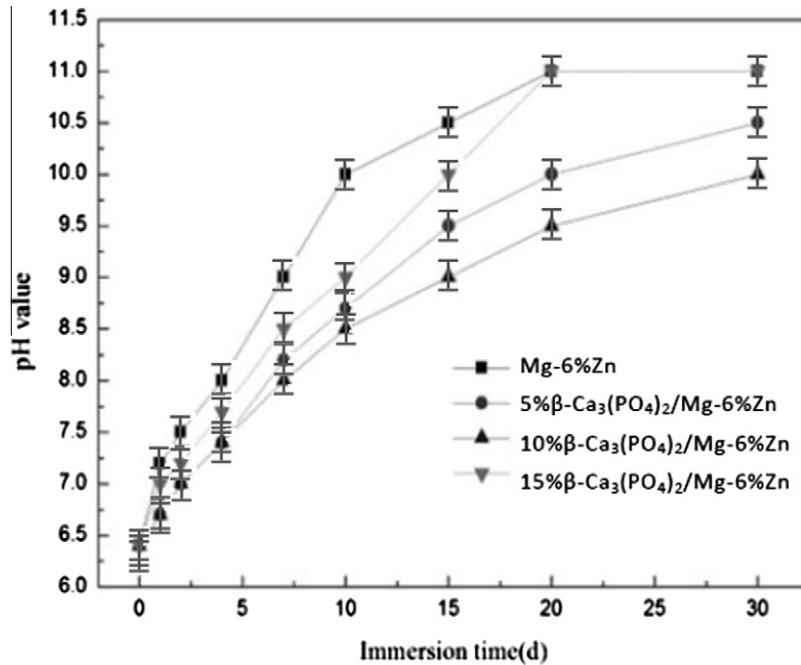


Fig. 5. Variation in the SBF pH values after immersion of the specimens.

the sample surface was quickly covered by a precipitated layer of corrosion products, reducing the production of gas bubbles. The accumulation of hydrogen bubbles around the magnesium composites will delay healing of the tissue and result in a pH increase. Monitoring the hydrogen evolution during immersion testing showed that the hydrogen production rates of the MMC specimens ( $\sim 3\text{--}5\text{ ml cm}^{-2}\text{ day}^{-1}$ ) were much lower than that of the Mg-6% Zn alloy ( $>25\text{ ml cm}^{-2}\text{ day}^{-1}$ ), as shown in Fig. 4.

This immersion test showed that the addition of 5 or 10%  $\beta$ -Ca<sub>3</sub>(PO<sub>4</sub>)<sub>2</sub> particles to the magnesium results in the lowest corrosion

rates. Obviously, high corrosion rates result in the rapid release of degradation products, and such a high rate of degradation under physiological conditions can cause a reduction in the mechanical integrity of the magnesium implant materials before the bone or tissue has healed sufficiently. Therefore, controlling the corrosion rate by the appropriate addition of  $\beta$ -Ca<sub>3</sub>(PO<sub>4</sub>)<sub>2</sub> particles is important in designing magnesium composites with optimal degradation properties.

Another important measurement is the variation in the SBF pH after corrosion of the  $\beta$ -Ca<sub>3</sub>(PO<sub>4</sub>)<sub>2</sub>/Mg-6% Zn composites. Increased

**Table 2**  
Parameters of the Mg–6% Zn and  $\beta$ -Ca<sub>3</sub>(PO<sub>4</sub>)<sub>2</sub>/Mg–6% Zn MMCs from polarization curves.

Material	Corrosion potential (V)	Corrosion current (A/cm <sup>2</sup> )	Corrosion rate (mg cm <sup>-2</sup> day <sup>-1</sup> )
5% $\beta$ -Ca <sub>3</sub> (PO <sub>4</sub> ) <sub>2</sub> /Mg–6% Zn	-1.3963	$2.0142 \times 10^{-4}$	6.90
10% $\beta$ -Ca <sub>3</sub> (PO <sub>4</sub> ) <sub>2</sub> /Mg–6% Zn	-1.4414	$2.7034 \times 10^{-4}$	7.85
15% $\beta$ -Ca <sub>3</sub> (PO <sub>4</sub> ) <sub>2</sub> /Mg–6% Zn	-1.5736	$4.2884 \times 10^{-4}$	9.35
Mg–6% Zn	-1.6011	$4.5347 \times 10^{-4}$	17.12

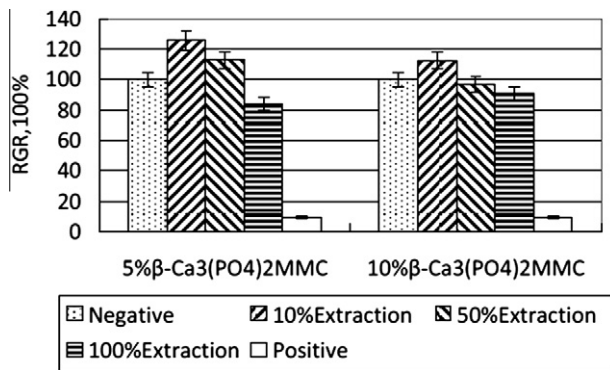


**Fig. 6.** RGRs of the L-929 cells cultured in different extracts of the MMCs.  $P > 0.05$ .

pH would cause local alkalization and disturb pH-dependent physiological processes in the vicinity of the composite. Fig. 5 shows the variation in pH of the SBF as a function of the immersion time. The pH value rises from a starting value of 6.5 to a maximum of approximately 11 on day 30 after immersion of the Mg–6% Zn alloy or the 15%  $\beta$ -Ca<sub>3</sub>(PO<sub>4</sub>)<sub>2</sub>/Mg–6% Zn composite. The pH increases slowly during the immersion test for the 10%  $\beta$ -Ca<sub>3</sub>(PO<sub>4</sub>)<sub>2</sub>/Mg–6% Zn specimens, reaching a value of 9.9 after 30 days.

### 3.2.2. Electrochemical testing

To more precisely evaluate the corrosion behavior of the  $\beta$ -Ca<sub>3</sub>(PO<sub>4</sub>)<sub>2</sub>/Mg–6% Zn MMCs electrochemical testing was performed to measure the short-term corrosion properties of the samples. The measured and calculated potentiodynamic polarization parameters of the three MMC samples and the Mg–6% Zn alloy are presented in Table 2. The results show an apparent difference in the corrosion potentials and the corrosion currents of the different specimens. The corrosion potential of the Mg–6% Zn alloy is the most negative of all of the specimens. The corrosion potential results indicate the existence of a protective film on the surface of the Mg alloy samples, and the higher potentials of the three  $\beta$ -Ca<sub>3</sub>(PO<sub>4</sub>)<sub>2</sub>/Mg–6% Zn MMCs indicate that the films on the MMCs are much more protective than those on the Mg–6% Zn alloy sample.

The short-term polarization measurements show corrosion rates that are higher than the corrosion rates determined in the immersion test. The differences in the rates measured by electrochemical testing and the immersion testing result from the greater number of parameters that influence the corrosion behavior of the  $\beta$ -Ca<sub>3</sub>(PO<sub>4</sub>)<sub>2</sub>/Mg–6% Zn MMCs during the short-term corrosion test. For example, the corrosion products on the surface of the specimens retard corrosion and play a more important role during the longer term immersion tests. In the electrochemical testing the corrosion products are removed from the surface of the samples by continuous hydrogen generation. The hydrogen evolution rate is proportional to the Mg dissolution or corrosion rate. In the immersion testing hydrogen evolution can only be observed at the beginning of the test. With increasing amounts of corrosion products on the surface the hydrogen evolution rate decreases

quickly, therefore, the corrosion reaction products have important effects on the degradation behavior of the experimental  $\beta$ -Ca<sub>3</sub>(PO<sub>4</sub>)<sub>2</sub>/Mg–6% Zn MMCs. On the basis of the evaluation of the mechanical properties, microstructure and in vitro corrosion behavior of three experimental MMCs, the 10%  $\beta$ -Ca<sub>3</sub>(PO<sub>4</sub>)<sub>2</sub>/Mg–6% Zn sample was selected for the following cytotoxicity assessments and in vivo biocompatibility testing.

### 3.3. Cytocompatibility testing

According to the above investigations, the 5% and 10%  $\beta$ -Ca<sub>3</sub>(PO<sub>4</sub>)<sub>2</sub>/Mg–6% Zn composites demonstrate appropriate in vitro corrosion properties in SBF. Thus they were selected as the objects of investigation in cytocompatibility tests. Cytocompatibility tests using an MTT assay have been used to determine the cytotoxicity of cobalt and chromium metal ions and composite materials [12]. Therefore, cytotoxicity tests on two experimental  $\beta$ -Ca<sub>3</sub>(PO<sub>4</sub>)<sub>2</sub>/Mg–6% Zn MMCs was performed to evaluate the in vitro biocompatibility of the materials. In this experiment L-929 cells were cultured in different extracts with concentrations of 100, 50 and 10%. The L929 cells can adhere, proliferate and survive in all three of these extracts in a cell culture system. The RGRs of the L-929 cells are shown in Fig. 6. The results show that the cells in different extracts were normal and healthy, and the results were similar to those of the negative control. Quantitatively, there were no significant differences between the RGRs of the cells in the extracts and those in the negative control. According to the ISO 10993-5:1999 standard, which focuses on cytocompatibility and quantifies the toxicity level of implants, the cytotoxicity of these extracts of MMCs was grade 0–1. Thus, the 5 and 10%  $\beta$ -Ca<sub>3</sub>(PO<sub>4</sub>)<sub>2</sub>/Mg–6% Zn composites are innocuous and are suitable for cellular applications.

### 3.4. In vivo degradation and biocompatibility testing

The surgical incisions in the Zelanian rabbits healed approximately 1 week post-operatively. The rabbits lived and moved freely in their cages for 12 weeks. The concentration variations of Mg<sup>2+</sup>, Zn<sup>2+</sup>, Ca<sup>2+</sup> ions in the Zelanian rabbit venous blood were measured and are shown in Fig. 7. The concentrations of these three ions in the blood were all in the normal ranges, as indicated in Fig. 7. The concentrations of Mg<sup>2+</sup> and Ca<sup>2+</sup> reached their maximum values in approximately 15 days and decreased to pre-operative levels after approximately 12 weeks. The concentration of Zn<sup>2+</sup> was steady over the entire course of the experiment. Such a phenomenon indicates that the metal ions that were biodegraded from the experimental 10%  $\beta$ -Ca<sub>3</sub>(PO<sub>4</sub>)<sub>2</sub>/Mg–6% Zn composite can be metabolized in the animal's blood and had no adverse effect on the animal.

The histopathological observations of the heart, liver, kidney and muscle tissues of the rabbits after 12 weeks are shown in Fig. 8. All of the tissues were normal, which suggests good in vivo biocompatibility of the 10%  $\beta$ -Ca<sub>3</sub>(PO<sub>4</sub>)<sub>2</sub>/Mg–6% Zn composite and that the degradation of such a composite does no harm to these important visceral organs.

The micro-CT micrographs of the bone fractures and the implanted MMCs are shown in Fig. 9. The experimental composite

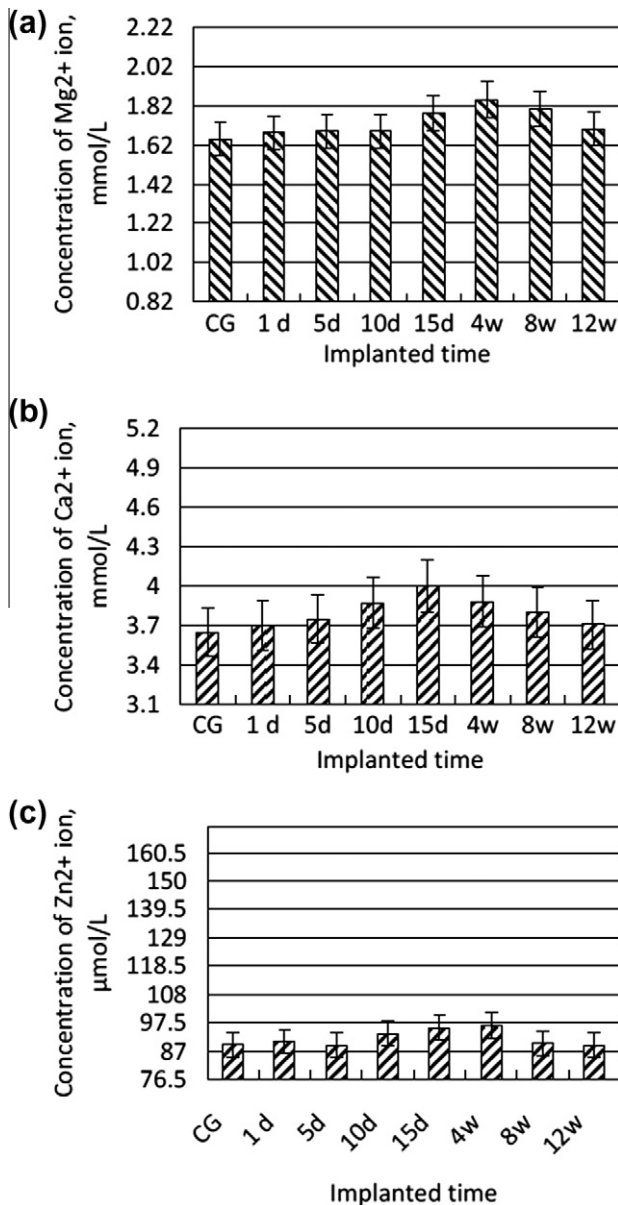


**Fig. 7.** The concentration variations of metal ions in the venous blood of rabbits after implanting the composites. (a) Variations in Mg<sup>2+</sup> (normal range 0.82–2.22 mmol l<sup>-1</sup>). (b) Variations in Ca<sup>2+</sup> (normal range 3.1–5.2 mmol l<sup>-1</sup>). (c) Variations in Zn<sup>2+</sup> (normal range 76.5–170 μmol l<sup>-1</sup>).

splints and screws are clearly visible after surgery and maintain their integrity 2 weeks post-operation (Fig. 9a). The 10% β-Ca<sub>3</sub>(PO<sub>4</sub>)<sub>2</sub>/Mg–6% Zn composite implant showed obvious degradation after 4 weeks; the edges of the composite implant become visibly fuzzy (Fig. 9b). After 8 weeks the implant composite splints and screws degraded and some bubbles appeared (Fig. 9c). The prefabricated fracture had healed and new bone tissues around the implant can be observed. The subcutaneous bubbles or those around the implant were produced during degradation of the composite, but such gas bubbles disappeared gradually after 8 weeks and no adverse effects on the rabbits were observed, consistent with the results reported in the literature [8]. The new bone tissue surrounding the implant increased with gradual degradation of the composite. After 12 weeks the residual implant became small and blurry (Fig. 9d), and new bone formation surrounding the implant showed that the composite improved concrescence of the bone tissues. No obvious inflammation response was observed throughout

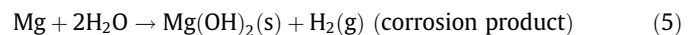
the entire degradation process, despite the presence of hydrogen bubbles. Fig. 10 shows the response of the bone tissue to the 10% β-Ca<sub>3</sub>(PO<sub>4</sub>)<sub>2</sub>/Mg–6% Zn implant at 4, 8 and 12 weeks post-implantation. There are newly formed fibrous connective tissues and osteoblasts around the prefabricated bone fracture. The trabeculae had obviously formed and the fibrous tissue was reduced after 8 weeks. The newly formed bone replaced the fibrous connective tissue after 12 weeks and the trabeculae were neatly distributed.

#### 4. Discussion

The β-Ca<sub>3</sub>(PO<sub>4</sub>)<sub>2</sub>/Mg–6% Zn composite implants exhibited good in vivo biocompatibility in rabbits because of their appropriate corrosion properties. The in vitro corrosion tests demonstrated that the 10% β-Ca<sub>3</sub>(PO<sub>4</sub>)<sub>2</sub>/Mg–6% Zn composite yielded the optimum synthetic properties, and it was selected for the analysis of degradation effects in vivo. As mentioned above in the test results, hydrogen gas was one of the corrosion products that affected the corrosion process and the tissues around the implanted composite in the rabbits. Other corrosion products on the surface of the specimens also influenced the degradation process of the 10% β-Ca<sub>3</sub>(PO<sub>4</sub>)<sub>2</sub>/Mg–6% Zn composite in vivo. The in vitro and in vivo corrosion products were compared to analyze their effects.

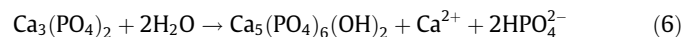
A cross-sectional view of the typical corrosion morphology of the 10% β-Ca<sub>3</sub>(PO<sub>4</sub>)<sub>2</sub>/Mg–6% Zn MMCs in SBF is shown in Fig. 11a. Non-uniform corrosion was observed for the MMC because the Mg matrix, MgZn phase and β-Ca<sub>3</sub>(PO<sub>4</sub>)<sub>2</sub> particles exhibited different corrosion properties in SBF. Corrosion product element analysis by X-ray spectroscopy (EDX) indicated that the white region (point A in Fig. 11a) contained many chemical elements that are corrosion products of Mg, the MgZn phase and β-Ca<sub>3</sub>(PO<sub>4</sub>)<sub>2</sub> particles. Fig. 11c shows X-ray phase identification of the corrosion products; the main constituents of the corrosion product surface layer are Mg(OH)<sub>2</sub>, CaCO<sub>3</sub> and hydroxyapatite (HA).

The corrosion reactions of the β-Ca<sub>3</sub>(PO<sub>4</sub>)<sub>2</sub>/Mg–6% Zn composite in SBF are analyzed in the following discussion. The magnesium matrix undergoes a chemical reaction with water, which releases hydrogen [24]:



Mg(OH)<sub>2</sub> is the main solid corrosion product produced by the reaction. The presence of this solid can impede corrosion penetration into the Mg matrix, but the high concentration of chloride ions can accelerate the corrosion rate by transforming Mg(OH)<sub>2</sub> into the more soluble MgCl<sub>2</sub>. Breakdown of the Mg(OH)<sub>2</sub> layer decreases the protected area on the surface of the specimen, consequently promoting further dissolution of the substrate. Makar and Kruger [24] showed that chloride ions participate in dissolution of the Mg matrix by accelerating the electrochemical reaction from magnesium to univalent magnesium ions.

The addition of β-Ca<sub>3</sub>(PO<sub>4</sub>)<sub>2</sub> to the Mg–6% Zn alloy significantly affected the corrosion rate of the MMC. β-Ca<sub>3</sub>(PO<sub>4</sub>)<sub>2</sub> reacts with the H<sub>2</sub>O in the body fluids to form Ca<sub>5</sub>(PO<sub>4</sub>)<sub>6</sub>(OH)<sub>2</sub>, which is beneficial to new bone growth. The reaction occurs as follows [25]:



The Ca<sub>5</sub>(PO<sub>4</sub>)<sub>6</sub>(OH)<sub>2</sub> produced on the surface of the β-Ca<sub>3</sub>(PO<sub>4</sub>)<sub>2</sub>/Mg–6% Zn composite is chemically stable and can impede the corrosion process, providing an appropriate pH-dependent physiological environment. The decomposition of β-Ca<sub>3</sub>(PO<sub>4</sub>)<sub>2</sub> during the

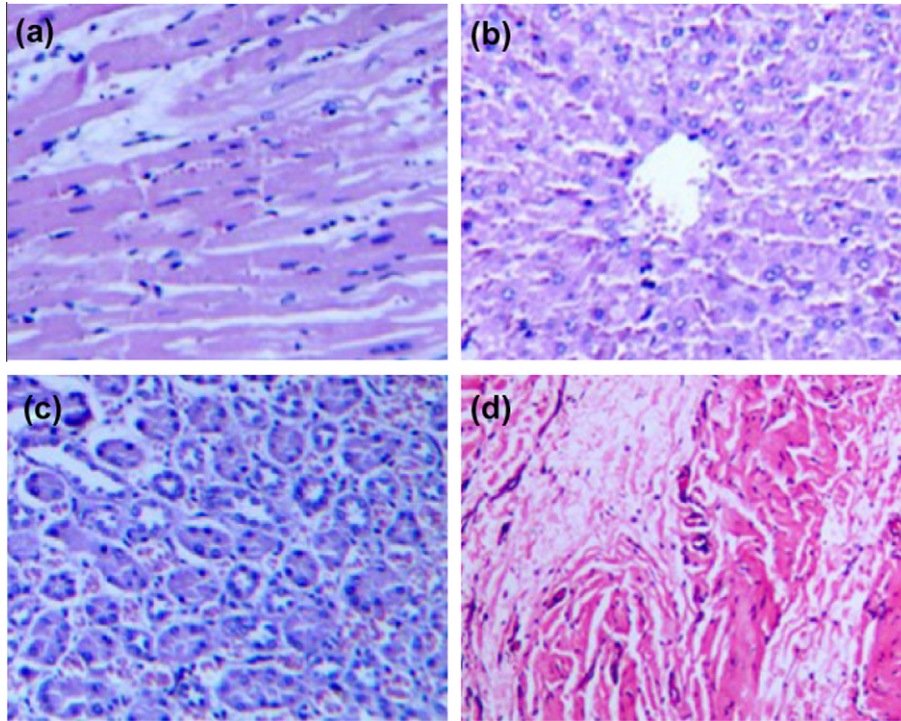


Fig. 8. Hematoxylin and eosin (HE) stained slices of (a) heart, (b) liver, (c) kidney and (d) muscle tissues.

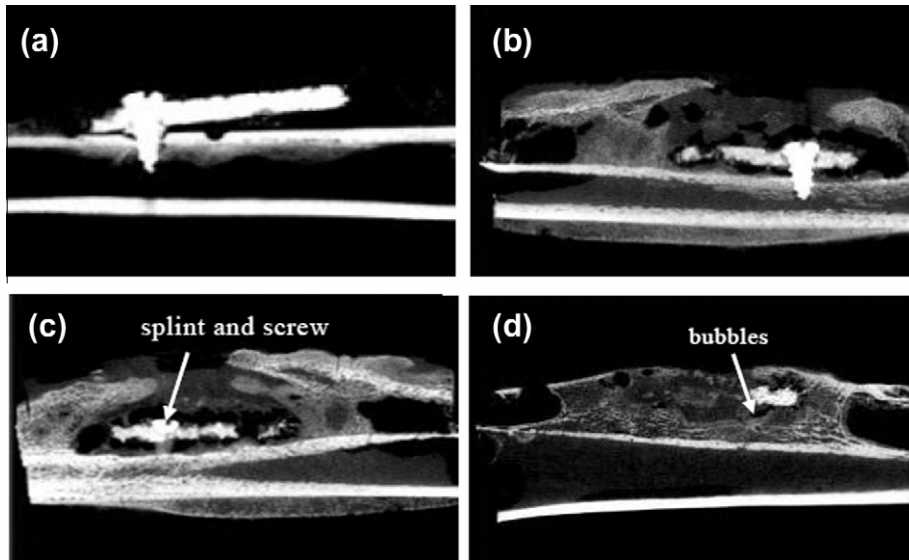


Fig. 9. Micro-CT micrographs taken (a) 2 weeks, (b) 4 weeks, (c) 8 weeks and (d) 12 weeks post-operation.

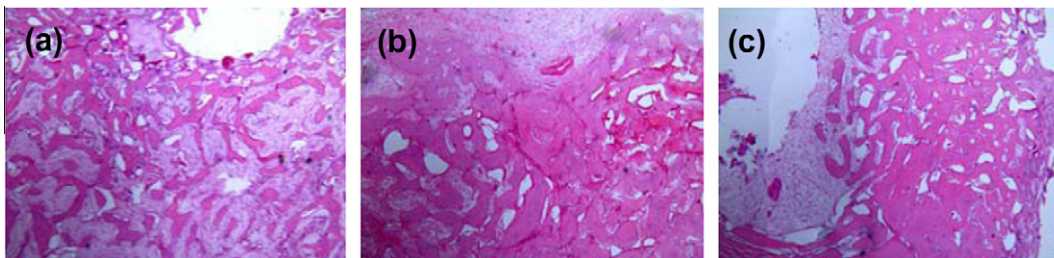


Fig. 10. HE stained bone tissues taken (a) 4, (b) 8 and (c) 12 weeks after implantation.

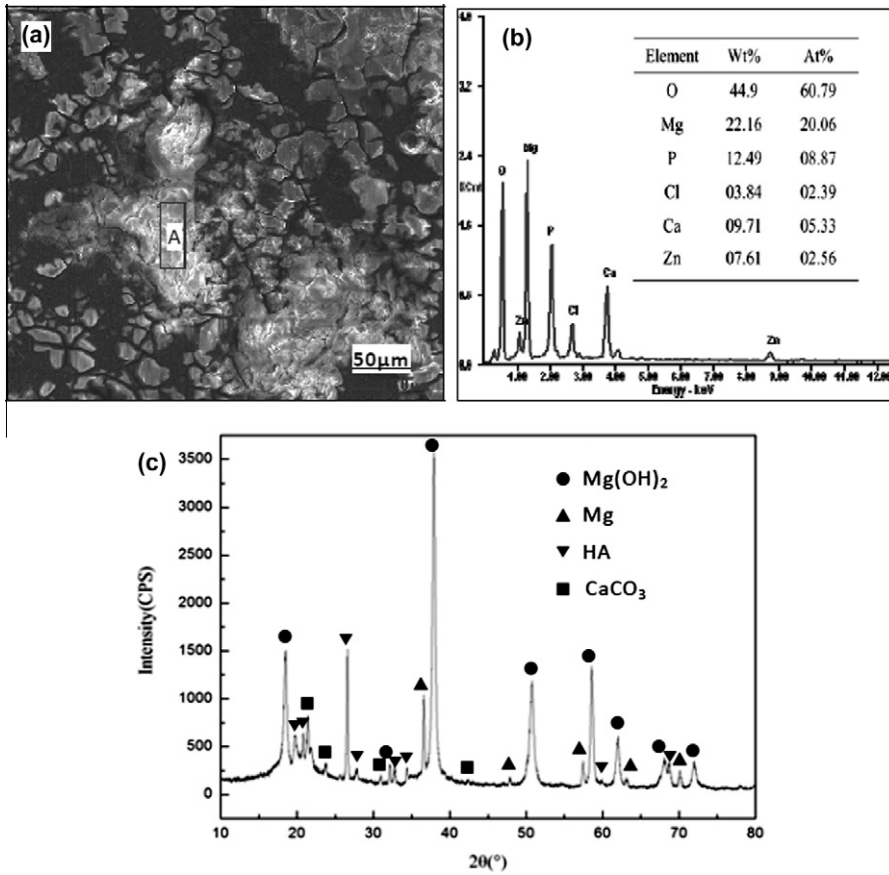


Fig. 11. Corrosion products of the 10%  $\beta$ -Ca<sub>3</sub>(PO<sub>4</sub>)<sub>2</sub>/Mg-6% Zn MMCs in SBF. (a) Morphology, (b) composition analysis and (c) X-ray phase identification.

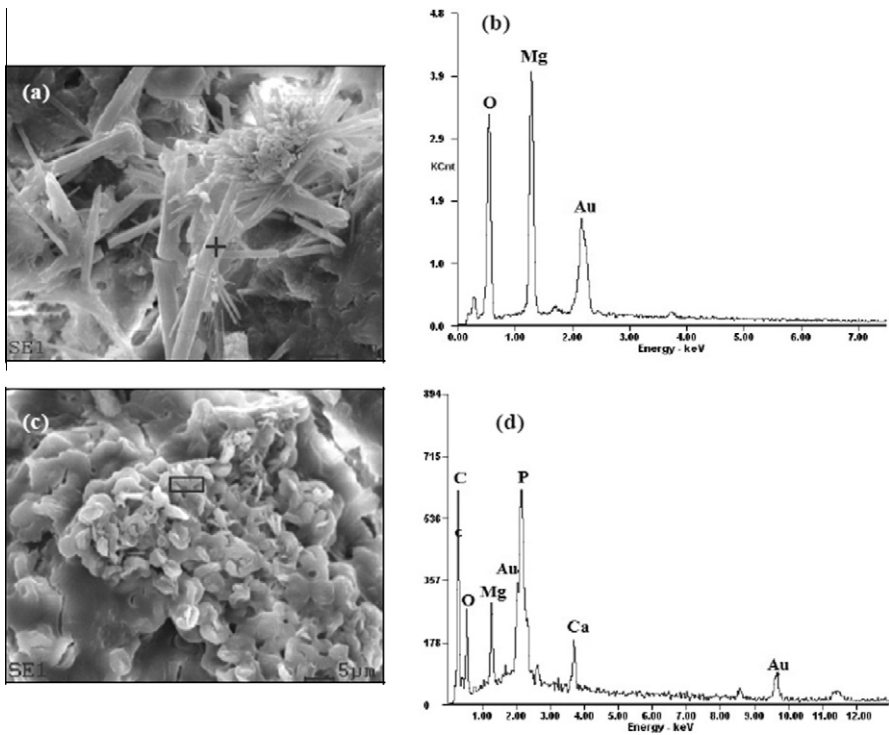
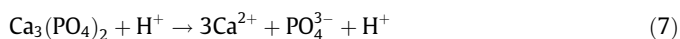


Fig. 12. The surface morphology and compositions of the residual composites after in vivo testing.

corrosion process can produce  $\text{HPO}_4^{2-}$ , which can effectively slow down the dissolution of magnesium because of the formation of compact and insoluble phosphates, although the concentration of  $\text{HPO}_4^{2-}$  is quite low in SBF. Unlike  $\text{Mg}(\text{OH})_2$ , such precipitated phosphates cannot be dissolved by chloride ions. The increasing concentration of  $\beta\text{-Ca}_3(\text{PO}_4)_2$  in the magnesium matrix can also cause a corrosion reaction because  $\beta\text{-Ca}_3(\text{PO}_4)_2$  can be dissolved by  $\text{H}^+$ . The reaction can be written as follows [25]:



This degradation reaction accelerates corrosion of the MMC, and the number of  $\beta\text{-Ca}_3(\text{PO}_4)_2$  particles in the magnesium matrix must be chosen so as to balance the corrosion reaction.

It is possible for  $\text{CaCO}_3$  to be formed by  $\text{CO}_2$  dissolved in the solution. The concentration of  $\text{HCO}_3^-$  at the corrosion sites and the  $\text{Ca}^{2+}$  ions produced by the decomposition of  $\beta\text{-Ca}_3(\text{PO}_4)_2$  contribute to the formation of insoluble carbonates ( $\text{CaCO}_3$ ), which suppress the spreading of corrosion at these sites. The combined result of these processes is the better corrosion resistance observed in the  $\beta\text{-Ca}_3(\text{PO}_4)_2/\text{Mg-6\% Zn}$  MMCs relative to the  $\text{Mg-6\% Zn}$  alloy.

The corrosion products of the implanted 10%  $\beta\text{-Ca}_3(\text{PO}_4)_2/\text{Mg-6\% Zn}$  had almost been absorbed and were barely detectable when the rabbits were killed 12 weeks post-operatively. Thus the residual implanted MMCs were observed and identified by SEM after 8 weeks. The surface morphologies and compositions of the residual MMCs are shown in Fig. 12. The surface of the implant was covered with a thick layer of corrosion products that exhibited different morphologies. One of the corrosion products exhibited an acicular shape, as shown in Fig. 12a. EDX revealed that it contained Mg and O, indicating  $\text{Mg}(\text{OH})_2$ , the main corrosion product of the matrix. The other corrosion product, with large amounts of Mg, Ca, P, O and C (Fig. 12b), was attributed to corrosion of the Mg matrix and  $\beta\text{-Ca}_3(\text{PO}_4)_2$ . However, it is obvious that the morphologies and compositions of the corrosion products from the in vitro and in vivo degradation experiments were different. The corrosion products in the in vitro SBF solution were relatively simple and easily identified. However, the in vivo degradation products were more complex because of the surrounding organic components, such as proteins and cells. The different morphologies and compositions found in vitro and in vivo suggest that degradation of the MMCs is greatly influenced by the surrounding environment. Thus, if the MMC implant is used in different parts of the body a variety of possible degradation behaviors should be considered. However, the results of the in vitro and in vivo testing suggest that these experimental MMCs have good biocompatibility for bone. The in vitro cytotoxicity of the MMC was found to be grade  $\sim 0-1$ , which indicated that such an MMC is safe as an implantable material. And because the corrosion product layer on the surface of the MMC could enhance osteoblast activity without harming the adjacent bone tissue, the MMC is actually helpful to newly formed bone surrounding the implants. The excess ions produced by degradation of the MMC can be excreted by normal metabolism with no kidney, liver or heart effects during the degradation process. Although bubbles from the corrosion products are observed during degradation, these can be controlled by decreasing the corrosion rate by adjusting the composition of the MMC. In summary, the MMCs are good candidates for implanted materials because of their good properties and biocompatibility.

## 5. Conclusions

1.  $\beta\text{-Ca}_3(\text{PO}_4)_2/\text{Mg-6\% Zn}$  composites can be sintered under vacuum by the powder metallurgy method.  $\alpha\text{-Mg}$ ,  $\text{MgZn}$  and  $\beta\text{-Ca}_3(\text{PO}_4)_2$  phases were identified in such sintered MMCs.

2. The mechanical properties and corrosion behavior show that the  $\beta\text{-Ca}_3(\text{PO}_4)_2/\text{Mg-6\% Zn}$  composite is suitable for implant applications. The 5 and 10%  $\beta\text{-Ca}_3(\text{PO}_4)_2/\text{Mg-6\% Zn}$  composites provide acceptable densities, strengths, elastic moduli and corrosion resistance in SBF at 37 °C. The densities and elastic moduli of the  $\beta\text{-Ca}_3(\text{PO}_4)_2/\text{Mg-6\% Zn}$  composites match those of natural bone, and the strengths were approximately twice that of natural bone. The 10%  $\beta\text{-Ca}_3(\text{PO}_4)_2/\text{Mg-6\% Zn}$  composite exhibited good corrosion resistance in SBF at 37 °C in both immersion tests and electrochemical measurements.
3. A grade of  $\sim 0-1$  for the in vitro cytotoxicity towards L-929 cells indicates that the  $\beta\text{-Ca}_3(\text{PO}_4)_2/\text{Mg-Zn}$  composite is safe for cellular applications.
4. In vivo testing indicates that the  $\beta\text{-Ca}_3(\text{PO}_4)_2/\text{Mg-6\% Zn}$  composite exhibits good biocompatibility with the tissue and the important visceral organs the heart, kidney and liver of rabbits.
5. The composite has a suitable degradation rate and improves the concrescence of pre-broken bone tissues. Over the course of the degradation process no obvious inflammation response could be observed, even in the presence of hydrogen bubbles, which are one of the corrosion products of  $\beta\text{-Ca}_3(\text{PO}_4)_2/\text{Mg-6\% Zn}$  composite degradation. Other corrosion products, such as  $\text{Mg}(\text{OH})_2$  and  $\text{Ca}_5(\text{PO}_4)_6(\text{OH})_2$ , can improve the biocompatibility and corrosion resistance of  $\beta\text{-Ca}_3(\text{PO}_4)_2/\text{Mg-Zn}$  composites.

## Appendix A. Figures with essential colour discrimination

Certain figures in this article, particularly Figures 5, 8 and 10, are difficult to interpret in black and white. The full colour images can be found in the on-line version, at <http://dx.doi.org/10.1016/j.actbio.2012.04.009>.

## References

- [1] Guelcher SA, Hollinger JO. An introduction to biomaterials. Boca Raton, FL: CRC Press; 2006. pp. 11–74.
- [2] Davis JR. Handbook of materials for medical devices. Materials Park, OH: ASM International; 2006. pp. 136–181.
- [3] Basu B, Katti D, Kumar A. Advanced biomaterials fundamentals, processing and applications. Hoboken, NJ: John Wiley & Sons; 2009. pp. 12–45.
- [4] Niinomi M. Recent metallic materials for biomedical applications. *Met Mater Trans A* 2002;33:477–86.
- [5] Heublein B, Rohde R, Kaese V, Niemeyer M, Hartung W, Haverich A. Biocorrosion of magnesium alloys: a new principle in cardiovascular implant technology? *Heart* 2003;89:651–6.
- [6] Witte F, Kaese V, Haferkamp H, Switzer E, Meyer Lindenberg A, Wirth CJ. In vivo corrosion of four magnesium alloys and the associated bone response. *Biomaterials* 2005;26:3557–63.
- [7] Song GL, Song SZ. A possible biodegradable magnesium implant material. *Adv Eng Mater* 2007;9:298–302.
- [8] Staiger MP, Pietak AM, Huadmai J, Dias G. Magnesium and its alloys as orthopedic biomaterials: a review. *Biomaterials* 2006;27:1728–34.
- [9] Xu ZG, Linford J, Chen S, Smith C, Sankar J. Preparation and characterization of porous magnesium alloys in biomedical applications. In: Proceedings of the ASME 2009 international mechanical engineering congress and exposition (IMECE2009), New York:ASME; 2009. p. 37–41.
- [10] Zeng R, Dietzel W, Witte F, Hort N, Blawert C. Progress and challenge for magnesium alloys as biomaterials. *Adv Eng Mater* 2008;10:B3–B14.
- [11] Zhang SX, Zhang XN, Zhao CL, Li JA, Song Y, Xie CY. Research on an Mg–Zn alloy as a degradable biomaterial. *Acta Biomater* 2010;6:626–40.
- [12] Seal CK, Vince K, Hodgson MA. Biodegradable surgical implants based on magnesium alloys – a review of current research. *Process Microstruct Performance Mater* 2009;4:1–4.
- [13] Song GL. Control of biodegradation of biocompatible magnesium alloys. *Corrosion Sci* 2007;49:1696–701.
- [14] Li ZJ, Gu XN, Lou SQ, Zheng Y. The development of binary MgCa alloys for use as biodegradable materials within bone. *Biomaterials* 2008;29:1329–44.
- [15] Gu XN, Zheng Y, Cheng Y, Zhong SP, Xi TF. In vitro corrosion and biocompatibility of binary magnesium alloys. *Biomaterials* 2009;30:484–98.
- [16] Witte F, Fischer J, Nellesen J, Crostack HA, Kaese V, Pisch AK. In vitro and in vivo corrosion measurements of magnesium alloys. *Biomaterials* 2006;27:1013–8.

- [17] Brar HS, Platt MO, Sarntinoranont M, Martin PI, Manuel MV. Magnesium as a biodegradable and bioabsorbable material for medical implants. *JOM* 2009;61:31–4.
- [18] Witte F, Feyerabend F, Maier P, Fischer J, Stormer M, Blawert C. Biodegradable magnesium–hydroxyapatite metal matrix composites. *Biomaterials* 2007;28:2163–74.
- [19] Bourg H, Lisle A. *Biomaterials developments and applications*. New York: Nova Science Publishers; 2010. pp. 224–284.
- [20] Yamaguchi M, Oishi H, Suketa Y. Stimulatory effect of zinc on bone formation in tissue culture. *Biochem Pharmacol* 1987;36:4007–12.
- [21] Engin NÖ, Taş C. Preparation of porous  $\text{Ca}_{10}(\text{PO}_4)_6(\text{OH})_2$  and  $\beta\text{-Ca}_3(\text{PO}_4)_2$  bioceramics. *J Am Ceram Soc* 2004;83:1581–4.
- [22] Koelmans H. Low-temperature phase transitions in  $\beta\text{-Ca}_3(\text{PO}_4)_2$  and related compounds. *J Phys Chem Solids* 1959;11:172–3.
- [23] Gibson L, Ashby M. *Cellular solids: structure and properties*. Sydney: Pergamon Press; 1988. pp. 316–331.
- [24] Makar GL, Kruger J. Corrosion of magnesium. *Int Mater Rev* 1993;38:138–53.
- [25] Fulmer MT, Ison IC, Hankermayer CR, Constantz BR, Ros J. Measurements of the solubility and dissolution rates of several hydroxyapatites. *Biomaterials* 2002;3:751–5.